

Directional Limits on Persistent Gravitational Waves Using LIGO S5 Science Data

J. Abadie,²⁹ B. P. Abbott,²⁹ R. Abbott,²⁹ M. Abernathy,⁶⁶ T. Accadia,²⁷ F. Acernese,^{19a,19c} C. Adams,³¹ R. Adhikari,²⁹ P. Ajith,²⁹ B. Allen,^{2,78} G. S. Allen,⁵² E. Amador Ceron,⁷⁸ R. S. Amin,³⁴ S. B. Anderson,²⁹ W. G. Anderson,⁷⁸ F. Antonucci,^{22a} M. A. Arain,⁶⁵ M. C. Araya,²⁹ M. Aronsson,²⁹ K. G. Arun,^{11b} Y. Aso,²⁹ S. M. Aston,⁶⁴ P. Astone,^{22a} D. Atkinson,³⁰ P. Aufmuth,²⁸ C. Aulbert,² S. Babak,¹ P. Baker,³⁷ G. Ballardin,¹³ S. Ballmer,²⁹ D. Barker,³⁰ S. Barnum,³² F. Barone,^{19a,19c} B. Barr,⁶⁶ P. Barriga,⁷⁷ L. Barsotti,³² M. Barsuglia,⁴ M. A. Barton,³⁰ I. Bartos,¹² R. Bassiri,⁶⁶ M. Bastarrika,⁶⁶ J. Bauchrowitz,² Th. S. Bauer,^{41a} B. Behnke,¹ M. G. Beker,^{41a} A. Belletoile,²⁷ M. Benacquista,⁵⁹ A. Bertolini,² J. Betzwieser,²⁹ N. Beveridge,⁶⁶ P. T. Beyersdorf,⁴⁸ S. Bigotta,^{21a,21b} I. A. Bilenko,³⁸ G. Billingsley,²⁹ J. Birch,³¹ S. Birindelli,^{43a} R. Biswas,⁷⁸ M. Bitossi,^{21a} M. A. Bizouard,^{26a} E. Black,²⁹ J. K. Blackburn,²⁹ L. Blackburn,³² D. Blair,⁷⁷ B. Bland,³⁰ M. Blom,^{41a} C. Boccara,^{26b} O. Bock,² T. P. Bodiya,³² R. Bondarescu,⁵⁴ F. Bondu,^{43b} L. Bonelli,^{21a,21b} R. Bonnand,³³ R. Bork,²⁹ M. Born,² S. Bose,⁷⁹ L. Bosi,^{20a} B. Bouhou,⁴ M. Boyle,⁸ S. Braccini,^{21a} C. Bradaschia,^{21a} P. R. Brady,⁷⁸ V. B. Braginsky,³⁸ J. E. Brau,⁷¹ J. Breyer,² D. O. Bridges,³¹ A. Brillet,^{43a} M. Brinkmann,² V. Brisson,^{26a} M. Britzger,² A. F. Brooks,²⁹ D. A. Brown,⁵³ R. Budzyński,^{45b} T. Bulik,^{45c,45d} H. J. Bulten,^{41a,41b} A. Buonanno,⁶⁷ J. Burguet-Castell,⁷⁸ O. Burmeister,² D. Buskulic,²⁷ C. Buy,⁴ R. L. Byer,⁵² L. Cadonati,⁶⁸ G. Cagnoli,^{17a} J. Cain,⁵⁶ E. Calloni,^{19a,19b} J. B. Camp,³⁹ E. Campagna,^{17a,17b} P. Campsie,⁶⁶ J. Cannizzo,³⁹ K. Cannon,²⁹ B. Canuel,¹³ J. Cao,⁶¹ C. Capano,⁵³ F. Carbognani,¹³ S. Caride,⁶⁹ S. Caudill,³⁴ M. Cavaglià,⁵⁶ F. Cavalier,^{26a} R. Cavalieri,¹³ G. Cella,^{21a} C. Cepeda,²⁹ E. Cesarini,^{17b} T. Chalermongsak,²⁹ E. Chalkley,⁶⁶ P. Charlton,^{11a} E. Chassande-Mottin,⁴ S. Chelkowski,⁶⁴ Y. Chen,⁸ A. Chincarini,¹⁸ N. Christensen,¹⁰ S. S. Y. Chua,⁵ C. T. Y. Chung,⁵⁵ D. Clark,⁵² J. Clark,⁹ J. H. Clayton,⁷⁸ F. Cleva,^{43a} E. Coccia,^{23a,23b} C. N. Colacino,^{21a,21b} J. Colas,¹³ A. Colla,^{22a,22b} M. Colombini,^{22b} R. Conte,⁷³ D. Cook,³⁰ T. R. Corbitt,³² N. Cornish,³⁷ A. Corsi,^{22a} C. A. Costa,³⁴ J.-P. Coulon,^{43a} D. M. Coward,⁷⁷ D. C. Coyne,²⁹ J. D. E. Creighton,⁷⁸ T. D. Creighton,⁵⁹ A. M. Cruise,⁶⁴ R. M. Culter,⁶⁴ A. Cumming,⁶⁶ L. Cunningham,⁶⁶ E. Cuoco,¹³ K. Dahl,² S. L. Danilishin,³⁸ R. Dannenberg,²⁹ S. D'Antonio,^{23a} K. Danzmann,^{2,28} K. Das,⁶⁵ V. Dattilo,¹³ B. Daudert,²⁹ M. Davier,^{26a} G. Davies,⁹ A. Davis,¹⁴ E. J. Daw,⁵⁷ R. Day,¹³ T. Dayanga,⁷⁹ R. De Rosa,^{19a,19b} D. DeBra,⁵² J. Degallaix,² M. del Prete,^{21a,21c} V. Dergachev,²⁹ R. DeRosa,³⁴ R. DeSalvo,²⁹ P. Devanka,⁹ S. Dhurandhar,²⁵ L. Di Fiore,^{19a} A. Di Lieto,^{21a,21b} I. Di Palma,² M. Di Paolo Emilio,^{23a,23c} A. Di Virgilio,^{21a} M. Díaz,⁵⁹ A. Dietz,²⁷ F. Donovan,³² K. L. Dooley,⁶⁵ E. E. Doomes,⁵¹ S. Dorsher,⁷⁰ E. S. D. Douglas,³⁰ M. Drago,^{44c,44d} R. W. P. Drever,⁶ J. C. Driggers,²⁹ J. Dueck,² J.-C. Dumas,⁷⁷ T. Eberle,² M. Edgar,⁶⁶ M. Edwards,⁹ A. Effler,³⁴ P. Ehrens,²⁹ R. Engel,²⁹ T. Etzel,²⁹ M. Evans,³² T. Evans,³¹ V. Fafone,^{23a,23b} S. Fairhurst,⁹ Y. Fan,⁷⁷ B. F. Farr,⁴² D. Fazi,⁴² H. Fehrmann,² D. Feldbaum,⁶⁵ I. Ferrante,^{21a,21b} F. Fidecaro,^{21a,21b} L. S. Finn,⁵⁴ I. Fiori,¹³ R. Flaminio,³³ M. Flanigan,³⁰ K. Flasch,⁷⁸ S. Foley,³² C. Forrest,⁷² E. Forisi,³¹ N. Fotopoulos,⁷⁸ J.-D. Fournier,^{43a} J. Franc,³³ S. Frasca,^{22a,22b} F. Frasconi,^{21a} M. Frede,² M. Frei,⁵⁸ Z. Frei,¹⁵ A. Freise,⁶⁴ R. Frey,⁷¹ T. T. Fricke,³⁴ D. Friedrich,² P. Fritschel,³² V. V. Frolov,³¹ P. Fulda,⁶⁴ M. Fyffe,³¹ M. Galimberti,³³ L. Gammaitoni,^{20a,20b} J. A. Garofoli,⁵³ F. Garufi,^{19a,19b} G. Gemme,¹⁸ E. Genin,¹³ A. Gennai,^{21a} I. Gholami,¹ S. Ghosh,⁷⁹ J. A. Giaime,^{34,31} S. Giampanis,² K. D. Giardina,³¹ A. Giazotto,^{21a} C. Gill,⁶⁶ E. Goetz,⁶⁹ L. M. Goggin,⁷⁸ G. González,³⁴ M. L. Gorodetsky,³⁸ S. Goßler,² R. Gouaty,²⁷ C. Graef,² M. Granata,⁴ A. Grant,⁶⁶ S. Gras,⁷⁷ C. Gray,³⁰ R. J. S. Greenhalgh,⁴⁷ A. M. Gretarsson,¹⁴ C. Greverie,^{43a} R. Grosso,⁵⁹ H. Grote,² S. Grunewald,¹ G. M. Guidi,^{17a,17b} E. K. Gustafson,²⁹ R. Gustafson,⁶⁹ B. Hage,²⁸ P. Hall,⁹ J. M. Hallam,⁶⁴ D. Hammer,⁷⁸ G. Hammond,⁶⁶ J. Hanks,³⁰ C. Hanna,²⁹ J. Hanson,³¹ J. Harms,⁶ G. M. Harry,³² I. W. Harry,⁹ E. D. Harstad,⁷¹ K. Haughian,⁶⁶ K. Hayama,⁴⁰ J.-F. Hayau,^{43b} T. Hayler,⁴⁷ J. Heefner,²⁹ H. Heitmann,^{43a} P. Hello,^{26a} I. S. Heng,⁶⁶ A. W. Heptonstall,²⁹ M. Hewitson,² S. Hild,⁶⁶ E. Hirose,⁵³ D. Hoak,⁶⁸ K. A. Hodge,²⁹ K. Holt,³¹ D. J. Hosken,⁶³ J. Hough,⁶⁶ E. J. Howell,⁷⁷ D. Hoyland,⁶⁴ D. Huet,¹³ B. Hughey,³² S. Husa,⁶² S. H. Huttner,⁶⁶ T. Huynh-Dinh,³¹ D. R. Ingram,³⁰ R. Inta,⁵ T. Isogai,¹⁰ A. Ivanov,²⁹ P. Jaranowski,^{45c} W. W. Johnson,³⁴ D. I. Jones,⁷⁵ G. Jones,⁹ R. Jones,⁶⁶ L. Ju,⁷⁷ P. Kalmus,²⁹ V. Kalogera,⁴² S. Kandhasamy,⁷⁰ J. B. Kanner,⁶⁷ E. Katsavounidis,³² K. Kawabe,³⁰ S. Kawamura,⁴⁰ F. Kawazoe,² W. Kells,²⁹ D. G. Keppel,²⁹ A. Khalaidovski,² F. Y. Khalili,³⁸ E. A. Khazanov,²⁴ H. Kim,² P. J. King,²⁹ D. L. Kinzel,³¹ J. S. Kissel,³⁴ S. Klimenko,⁶⁵ V. Kondrashov,²⁹ R. Kopparapu,⁵⁴ S. Koranda,⁷⁸ I. Kowalska,^{45c} D. Kozak,²⁹ T. Krause,⁵⁸ V. Kringel,² S. Krishnamurthy,⁴² B. Krishnan,¹ A. Królak,^{45a,45f} G. Kuehn,² J. Kullman,² R. Kumar,⁶⁶ P. Kwee,²⁸ M. Landry,³⁰ M. Lang,⁵⁴ B. Lantz,⁵² N. Lastzka,² A. Lazzarini,²⁹ P. Leaci,¹ J. Leong,² I. Leonor,⁷¹ N. Leroy,^{26a} N. Letendre,²⁷ J. Li,⁵⁹ T. G. F. Li,^{41a} N. Liguori,^{44a,44b} H. Lin,⁶⁵ P. E. Lindquist,²⁹ N. A. Lockerbie,⁷⁶ D. Lodhia,⁶⁴ M. Lorenzini,^{17a} V. Lorette,^{26b} M. Lormand,³¹ G. Losurdo,^{17a} P. Lu,⁵² J. Luan,⁸ M. Lubinski,³⁰ A. Lucianetti,⁶⁵ H. Lück,^{2,28} A. D. Lundgren,⁵³ B. Machenschalk,² M. MacInnis,³² M. Mageswaran,²⁹ K. Mailand,²⁹ E. Majorana,^{22a} C. Mak,²⁹ I. Maksimovic,^{26b}

N. Man,^{43a} I. Mandel,⁴² V. Mandic,⁷⁰ M. Mantovani,^{21a,21c} F. Marchesoni,^{20a} F. Marion,²⁷ S. Márka,¹² Z. Márka,¹² E. Maros,²⁹ J. Marque,¹³ F. Martelli,^{17a,17b} I. W. Martin,⁶⁶ R. M. Martin,⁶⁵ J. N. Marx,²⁹ K. Mason,³² A. Masserot,²⁷ F. Matichard,³² L. Matone,¹² R. A. Matzner,⁵⁸ N. Mavalvala,³² R. McCarthy,³⁰ D. E. McClelland,⁵ S. C. McGuire,⁵¹ G. McIntyre,²⁹ G. McIvor,⁵⁸ D. J. A. McKechnan,⁹ G. Meadors,⁶⁹ M. Mehmet,² T. Meier,²⁸ A. Melatos,⁵⁵ A. C. Melissinos,⁷² G. Mendell,³⁰ D. F. Menéndez,⁵⁴ R. A. Mercer,⁷⁸ L. Merrill,⁷⁷ S. Meshkov,²⁹ C. Messenger,² M. S. Meyer,³¹ H. Miao,⁷⁷ C. Michel,³³ L. Milano,^{19a,19b} J. Miller,⁶⁶ Y. Minenkov,^{23a} Y. Mino,⁸ S. Mitra,²⁹ V. P. Mitrofanov,³⁸ G. Mitselmakher,⁶⁵ R. Mittleman,³² B. Moe,⁷⁸ M. Mohan,¹³ S. D. Mohanty,⁵⁹ S. R. P. Mohapatra,⁶⁸ D. Moraru,³⁰ J. Moreau,^{26b} G. Moreno,³⁰ N. Morgado,³³ A. Morgia,^{23a,23b} T. Morioka,⁴⁰ K. Mors,² S. Mosca,^{19a,19b} V. Moscatelli,^{22a} K. Mossavi,² B. Mours,²⁷ C. M. Mow-Lowry,⁵ G. Mueller,⁶⁵ S. Mukherjee,⁵⁹ A. Mullavey,⁵ H. Müller-Ebhardt,² J. Munch,⁶³ P. G. Murray,⁶⁶ T. Nash,²⁹ R. Nawrodt,⁶⁶ J. Nelson,⁶⁶ I. Neri,^{20a,20b} G. Newton,⁶⁶ A. Nishizawa,⁴⁰ F. Nocera,¹³ D. Nolting,³¹ E. Ochsner,⁶⁷ J. O'Dell,⁴⁷ G. H. Ogin,²⁹ R. G. Oldenburg,⁷⁸ B. O'Reilly,³¹ R. O'Shaughnessy,⁵⁴ C. Osthelder,²⁹ D. J. Ottaway,⁶³ R. S. Ottens,⁶⁵ H. Overmier,³¹ B. J. Owen,⁵⁴ A. Page,⁶⁴ G. Pagliaroli,^{23a,23c} L. Palladino,^{23a,23c} C. Palomba,^{22a} Y. Pan,⁶⁷ C. Pankow,⁶⁵ F. Paoletti,^{21a,13} M. A. Papa,^{1,78} S. Pardi,^{19a,19b} M. Pareja,² M. Parisi,^{19b} A. Pasqualetti,¹³ R. Passaquieti,^{21a,21b} D. Passuello,^{21a} P. Patel,²⁹ D. Pathak,⁹ M. Pedraza,²⁹ L. Pekowsky,⁵³ S. Penn,¹⁶ C. Peralta,¹ A. Perreca,⁶⁴ G. Persichetti,^{19a,19b} M. Pichot,^{43a} M. Pickenpack,² F. Piergiovanni,^{17a,17b} M. Pietka,^{45e} L. Pinard,³³ I. M. Pinto,⁷⁴ M. Pitkin,⁶⁶ H. J. Pletsch,² M. V. Plissi,⁶⁶ R. Poggiani,^{21a,21b} F. Postiglione,⁷³ M. Prato,¹⁸ V. Predoi,⁹ L. R. Price,⁷⁸ M. Prijatelj,² M. Principe,⁷⁴ R. Prix,² G. A. Prodi,^{44a,44b} L. Prokhorov,³⁸ O. Puncken,² M. Punturo,^{20a} P. Puppo,^{22a} V. Quetschke,⁵⁹ F. J. Raab,³⁰ D. S. Rabeling,^{41a,41b} T. Radke,¹ H. Radkins,³⁰ P. Raffai,¹⁵ M. Rakhmanov,⁵⁹ B. Rankins,⁵⁶ P. Rapagnani,^{22a,22b} V. Raymond,⁴² V. Re,^{44a,44b} C. M. Reed,³⁰ T. Reed,³⁵ T. Regimbau,^{43a} S. Reid,⁶⁶ D. H. Reitze,⁶⁵ F. Ricci,^{22a,22b} R. Riesen,³¹ K. Riles,⁶⁹ P. Roberts,³ N. A. Robertson,^{29,66} F. Robinet,^{26a} C. Robinson,⁹ E. L. Robinson,¹ A. Rocchi,^{23a} S. Roddy,³¹ C. Röver,² L. Rolland,²⁷ J. Rollins,¹² J. D. Romano,⁵⁹ R. Romano,^{19a,19c} J. H. Romie,³¹ D. Rosińska,^{45g} S. Rowan,⁶⁶ A. Rüdiger,² P. Ruggi,¹³ K. Ryan,³⁰ S. Sakata,⁴⁰ M. Sakosky,³⁰ F. Salemi,² L. Sammut,⁵⁵ L. Sancho de la Jordana,⁶² V. Sandberg,³⁰ V. Sannibale,²⁹ L. Santamaría,¹ G. Santostasi,³⁶ S. Saraf,⁴⁹ B. Sassolas,³³ B. S. Sathyaprakash,⁹ S. Sato,⁴⁰ M. Satterthwaite,⁵ P. R. Saulson,⁵³ R. Savage,³⁰ R. Schilling,² R. Schnabel,² R. M. S. Schofield,⁷¹ B. Schulz,² B. F. Schutz,^{1,9} P. Schwinberg,³⁰ J. Scott,⁶⁶ S. M. Scott,⁵ A. C. Searle,²⁹ F. Seifert,²⁹ D. Sellers,³¹ A. S. Sengupta,²⁹ D. Sentenac,¹³ A. Sergeev,²⁴ D. A. Shaddock,⁵ B. Shapiro,³² P. Shawhan,⁶⁷ D. H. Shoemaker,³² A. Sibley,³¹ X. Siemens,⁷⁸ D. Sigg,³⁰ A. Singer,²⁹ A. M. Sintes,⁶² G. Skelton,⁷⁸ B. J. J. Slagmolen,⁵ J. Slutsky,³⁴ J. R. Smith,⁷ M. R. Smith,²⁹ N. D. Smith,³² K. Somiya,⁸ B. Sorazu,⁶⁶ F. C. Speirits,⁶⁶ L. Sperandio,^{23a,23b} A. J. Stein,³² L. C. Stein,³² S. Steinlechner,² S. Steplewski,⁷⁹ A. Stochino,²⁹ R. Stone,⁵⁹ K. A. Strain,⁶⁶ S. Strigin,³⁸ A. S. Stroeer,³⁹ R. Sturani,^{17a,17b} A. L. Stuver,³¹ T. Z. Summerscales,³ M. Sung,³⁴ S. Susmithan,⁷⁷ P. J. Sutton,⁹ B. Swinkels,¹³ G. P. Szokoly,¹⁵ D. Talukder,⁷⁹ D. B. Tanner,⁶⁵ S. P. Tarabrin,² J. R. Taylor,² R. Taylor,²⁹ P. Thomas,³⁰ K. A. Thorne,³¹ K. S. Thorne,⁸ E. Thrane,^{70,*} A. Thüring,²⁸ C. Titsler,⁵⁴ K. V. Tokmakov,^{66,76} A. Toncelli,^{21a,21b} M. Tonelli,^{21a,21b} O. Torre,^{21a,21c} C. Torres,³¹ C. I. Torrie,^{29,66} E. Tournefier,²⁷ F. Travasso,^{20a,20b} G. Traylor,³¹ M. Trias,⁶² J. Trummer,²⁷ K. Tseng,⁵² L. Turner,²⁹ D. Ugolini,⁶⁰ K. Urbanek,⁵² H. Vahlbruch,²⁸ B. Vaishnav,⁵⁹ G. Vajente,^{21a,21b} M. Vallisneri,⁸ J. F. J. van den Brand,^{41a,41b} C. Van Den Broeck,⁹ S. van der Putten,^{41a} M. V. van der Sluys,⁴² A. A. van Veggel,⁶⁶ S. Vass,²⁹ R. Vaulin,⁷⁸ M. Vavoulidis,^{26a} A. Vecchio,⁶⁴ G. Vedovato,^{44c} J. Veitch,⁹ P. J. Veitch,⁶³ C. Veltkamp,² D. Verkindt,²⁷ F. Vetranò,^{17a,17b} A. Viceré,^{17a,17b} A. E. Villar,²⁹ J.-Y. Vinet,^{43a} H. Vocca,^{20a} C. Vorvick,³⁰ S. P. Vyachanin,³⁸ S. J. Waldman,³² L. Wallace,²⁹ A. Wanner,² R. L. Ward,²⁹ M. Was,^{26a} P. Wei,⁵³ M. Weinert,² A. J. Weinstein,²⁹ R. Weiss,³² L. Wen,^{8,77} S. Wen,³⁴ P. Wessels,² M. West,⁵³ T. Westphal,² K. Wette,⁵ J. T. Whelan,⁴⁶ S. E. Whitcomb,²⁹ D. White,⁵⁷ B. F. Whiting,⁶⁵ C. Wilkinson,³⁰ P. A. Willems,²⁹ L. Williams,⁶⁵ B. Willke,^{2,28} L. Winkelmann,² W. Winkler,² C. C. Wipf,³² A. G. Wiseman,⁷⁸ G. Woan,⁶⁶ R. Wooley,³¹ J. Worden,³⁰ I. Yakushin,³¹ H. Yamamoto,²⁹ K. Yamamoto,² D. Yeaton-Massey,²⁹ S. Yoshida,⁵⁰ P. Yu,⁷⁸ M. Yvert,²⁷ M. Zanolin,¹⁴ L. Zhang,²⁹ Z. Zhang,⁷⁷ C. Zhao,⁷⁷ N. Zotov,³⁵ M. E. Zucker,³² and J. Zweizig²⁹

(LIGO Scientific Collaboration)

(Virgo Collaboration)

¹Albert-Einstein-Institut, Max-Planck-Institut für Gravitationsphysik, D-14476 Golm, Germany²Albert-Einstein-Institut, Max-Planck-Institut für Gravitationsphysik, D-30167 Hannover, Germany³Andrews University, Berrien Springs, Michigan 49104, USA

- ⁴*Laboratoire AstroParticule et Cosmologie (APC) Université Paris Diderot, CNRS: IN2P3, CEA: DSM/IRFU, Observatoire de Paris 10, rue A.Domon et L.Duquet, 75013 Paris - France*
- ⁵*Australian National University, Canberra, ACT 0200, Australia*
- ⁶*California Institute of Technology, Pasadena, California 91125, USA*
- ⁷*California State University Fullerton, Fullerton California 92831, USA*
- ⁸*Caltech-CaRT, Pasadena, California 91125, USA*
- ⁹*Cardiff University, Cardiff, CF24 3AA, United Kingdom*
- ¹⁰*Carleton College, Northfield, Minnesota 55057, USA*
- ^{11a}*Charles Sturt University, Wagga Wagga, NSW 2678, Australia*
- ^{11b}*Chennai Mathematical Institute, Siruseri 603103 India*
- ¹²*Columbia University, New York, New York 10027, USA*
- ¹³*European Gravitational Observatory (EGO), I-56021 Cascina (PI), Italy*
- ¹⁴*Embry-Riddle Aeronautical University, Prescott, Arizona 86301, USA*
- ¹⁵*Eötvös Loránd University, Budapest, 1117 Hungary*
- ¹⁶*Hobart and William Smith Colleges, Geneva, New York 14456, USA*
- ^{17a}*INFN, Sezione di Firenze, I-50019 Sesto Fiorentino, Italy*
- ^{17b}*Università degli Studi di Urbino 'Carlo Bo', I-61029 Urbino, Italy*
- ¹⁸*INFN, Sezione di Genova; I-16146 Genova, Italy*
- ^{19a}*INFN, Sezione di Napoli, Italy*
- ^{19b}*Università di Napoli 'Federico II', Italy*
- ^{19c}*Complesso Universitario di Monte S.Angelo, I-80126 Napoli, Università di Salerno, Fisciano, I-84084 Salerno, Italy*
- ^{20a}*INFN, Sezione di Perugia, I-06123 Perugia, Italy*
- ^{20b}*Università di Perugia, I-06123 Perugia, Italy*
- ^{21a}*INFN, Sezione di Pisa, I-56127 Pisa, Italy*
- ^{21b}*Università di Pisa, I-56127 Pisa, Italy*
- ^{21c}*Università di Siena, I-53100 Siena, Italy*
- ^{22a}*INFN, Sezione di Roma, I-00185 Roma, Italy*
- ^{22b}*Università 'La Sapienza', I-00185 Roma, Italy*
- ^{23a}*INFN, Sezione di Roma Tor Vergata, Italy*
- ^{23b}*Università di Roma Tor Vergata, I-00133 Roma, Italy*
- ^{23c}*Università dell'Aquila, I-67100 L'Aquila, Italy*
- ²⁴*Institute of Applied Physics, Nizhny Novgorod, 603950, Russia*
- ²⁵*Inter-University Centre for Astronomy and Astrophysics, Pune - 411007, India*
- ^{26a}*LAL, Université Paris-Sud, IN2P3/CNRS, F-91898 Orsay, France*
- ^{26b}*ESPCI, CNRS, F-75005 Paris, France*
- ²⁷*Laboratoire d'Annecy-le-Vieux de Physique des Particules (LAPP), Université de Savoie, CNRS/IN2P3, F-74941 Annecy-Le-Vieux, France*
- ²⁸*Leibniz Universität Hannover, D-30167 Hannover, Germany*
- ²⁹*LIGO - California Institute of Technology, Pasadena, California 91125, USA*
- ³⁰*LIGO - Hanford Observatory, Richland, Washington 99352, USA*
- ³¹*LIGO - Livingston Observatory, Livingston, Louisiana 70754, USA*
- ³²*LIGO - Massachusetts Institute of Technology, Cambridge, Massachusetts 02139, USA*
- ³³*Laboratoire des Matériaux Avancés (LMA), IN2P3/CNRS, F-69622 Villeurbanne, Lyon, France*
- ³⁴*Louisiana State University, Baton Rouge, Louisiana 70803, USA*
- ³⁵*Louisiana Tech University, Ruston, Louisiana 71272, USA*
- ³⁶*McNeese State University, Lake Charles, Louisiana 70609, USA*
- ³⁷*Montana State University, Bozeman, Montana 59717, USA*
- ³⁸*Moscow State University, Moscow, 119992, Russia*
- ³⁹*NASA/Goddard Space Flight Center, Greenbelt, Maryland 20771, USA*
- ⁴⁰*National Astronomical Observatory of Japan, Tokyo 181-8588, Japan*
- ^{41a}*Nikhef, National Institute for Subatomic Physics, P.O. Box 41882, 1009 DB Amsterdam, The Netherlands*
- ^{41b}*VU University Amsterdam, De Boelelaan 1081, 1081 HV Amsterdam, The Netherlands*
- ⁴²*Northwestern University, Evanston, Illinois 60208, USA*
- ^{43a}*Université Nice-Sophia-Antipolis, CNRS, Observatoire de la Côte d'Azur, F-06304 Nice, France*
- ^{43b}*Institut de Physique de Rennes, CNRS, Université de Rennes 1, 35042 Rennes, France*
- ^{44a}*INFN, Gruppo Collegato di Trento, I-38050 Povo, Trento, Italy*
- ^{44b}*Università di Trento, I-38050 Povo, Trento, Italy,*
- ^{44c}*INFN, Sezione di Padova, I-35131 Padova, Italy*
- ^{44d}*Università di Padova, I-35131 Padova, Italy*
- ^{45a}*IM-PAN 00-956 Warsaw, Poland*

- ^{45b}Warsaw University 00-681 Warsaw, Poland
^{45c}Astronomical Observatory Warsaw University 00-478 Warsaw, Poland
^{45d}CAMK-PAN 00-716 Warsaw, Poland
^{45e}Białystok University 15-424 Białystok, Poland
^{45f}IPJ 05-400 Świerk-Otwock, Poland
^{45g}Institute of Astronomy 65-265 Zielona Góra, Poland
⁴⁶Rochester Institute of Technology, Rochester, New York 14623, USA
⁴⁷Rutherford Appleton Laboratory, HSIC, Chilton, Didcot, Oxon OX11 0QX United Kingdom
⁴⁸San Jose State University, San Jose, California 95192, USA
⁴⁹Sonoma State University, Rohnert Park, California 94928, USA
⁵⁰Southeastern Louisiana University, Hammond, Louisiana 70402, USA
⁵¹Southern University and A&M College, Baton Rouge, Louisiana 70813, USA
⁵²Stanford University, Stanford, California 94305, USA
⁵³Syracuse University, Syracuse, New York 13244, USA
⁵⁴The Pennsylvania State University, University Park, Pennsylvania 16802, USA
⁵⁵The University of Melbourne, Parkville VIC 3010, Australia
⁵⁶The University of Mississippi, University, Mississippi 38677, USA
⁵⁷The University of Sheffield, Sheffield S10 2TN, United Kingdom
⁵⁸The University of Texas at Austin, Austin, Texas 78712, USA
⁵⁹The University of Texas at Brownsville and Texas Southmost College, Brownsville, Texas 78520, USA
⁶⁰Trinity University, San Antonio, Texas 78212, USA
⁶¹Tsinghua University, Beijing 100084 China
⁶²Universitat de les Illes Balears, E-07122 Palma de Mallorca, Spain
⁶³University of Adelaide, Adelaide, SA 5005, Australia
⁶⁴University of Birmingham, Birmingham, B15 2TT, United Kingdom
⁶⁵University of Florida, Gainesville, Florida 32611, USA
⁶⁶University of Glasgow, Glasgow, G12 8QQ, United Kingdom
⁶⁷University of Maryland, College Park, Maryland 20742, USA
⁶⁸University of Massachusetts - Amherst, Amherst, Massachusetts 01003, USA
⁶⁹University of Michigan, Ann Arbor, Michigan 48109, USA
⁷⁰University of Minnesota, Minneapolis, Minnesota 55455, USA
⁷¹University of Oregon, Eugene, Oregon 97403, USA
⁷²University of Rochester, Rochester, New York 14627, USA
⁷³University of Salerno, I-84084 Fisciano (Salerno), Italy and INFN (Sezione di Napoli), Italy
⁷⁴University of Sannio at Benevento, I-82100 Benevento, Italy and INFN (Sezione di Napoli), Italy
⁷⁵University of Southampton, Southampton, SO17 1BJ, United Kingdom
⁷⁶University of Strathclyde, Glasgow, G1 1XQ, United Kingdom
⁷⁷University of Western Australia, Crawley, WA 6009, Australia
⁷⁸University of Wisconsin–Milwaukee, Milwaukee, Wisconsin 53201, USA
⁷⁹Washington State University, Pullman, Washington 99164, USA
(Received 9 October 2011; published 29 December 2011)

The gravitational-wave (GW) sky may include nearby pointlike sources as well as stochastic backgrounds. We perform two directional searches for persistent GWs using data from the LIGO S5 science run: one optimized for pointlike sources and one for arbitrary extended sources. Finding no evidence to support the detection of GWs, we present 90% confidence level (C.L.) upper-limit maps of GW strain power with typical values between $2 - 20 \times 10^{-50}$ strain² Hz⁻¹ and $5 - 35 \times 10^{-49}$ strain² Hz⁻¹ sr⁻¹ for pointlike and extended sources, respectively. The latter result is the first of its kind. We also set 90% C.L. limits on the narrow-band root-mean-square GW strain from interesting targets including Sco X-1, SN 1987A and the Galactic center as low as $\approx 7 \times 10^{-25}$ in the most sensitive frequency range near 160 Hz.

DOI: 10.1103/PhysRevLett.107.271102

PACS numbers: 95.85.Sz, 95.30.Sf, 97.60.Jd, 98.80.-k

Introduction.—One of the most ambitious goals of gravitational-wave (GW) astronomy is to measure the stochastic gravitational-wave background (SGWB), which can arise through a variety of mechanisms including am-

plification of vacuum fluctuations following inflation [1], phase transitions in the early Universe [2], cosmic strings [3] and pre-big bang models [4,5]. Astrophysical sources of the SGWB include the superposition of unresolved

sources such as core-collapse supernovae [6], neutron-star instabilities [7], binary mergers [8] and persistent emission from neutron stars [9].

We present the results of two analyses using data from the LIGO S5 science run: a radiometer analysis optimized for pointlike sources and a spherical-harmonic decomposition (SHD) analysis, which allows for arbitrary angular distributions. This work presents the first measurement of the GW sky in a framework consistent with an arbitrary extended source.

Detectors.—We analyze data from LIGO’s 4 and 2 km detectors (H1 and H2) in Hanford, WA and the 4 km detector (L1) in Livingston Parish, LA during the S5 science run (Nov. 5, 2005—Sep. 30, 2007). During S5, both H1 and L1 reached a strain sensitivity of 3×10^{-23} strain $\text{Hz}^{-1/2}$ in the most sensitive region between 100–200 Hz [10] and collected 331 days of coincident H1L1 and H2L1 data. S5 saw milestones including limits on GWs from the Crab pulsar surpassing those inferred from the Crab’s spindown [11], as well as limits on the isotropic SGWB surpassing indirect limits from big bang nucleosynthesis and the cosmic microwave background [12]. This work builds on [12,13].

Methodology.—Following [13,14] we present a framework for analyzing the angular distribution of GWs. We assume that the GW signal is stationary and unpolarized, but not necessarily isotropic. It follows that the GW energy density $\Omega_{\text{GW}}(f)$, can be expressed in terms of the GW power spectrum, $\mathcal{P}(f, \hat{\Omega})$:

$$\Omega_{\text{GW}}(f) \equiv \frac{f}{\rho_c} \frac{d\rho_{\text{GW}}}{df} = \frac{2\pi^2}{3H_0^2} f^3 \int_{S^2} d\hat{\Omega} \mathcal{P}(f, \hat{\Omega}). \quad (1)$$

Here f is frequency, $\hat{\Omega}$ is sky location, ρ_c is the critical density of the Universe and H_0 is Hubble’s constant. We further assume that $\mathcal{P}(f, \hat{\Omega})$ can be factored (in our analysis band) into an angular power spectrum, $\mathcal{P}(\hat{\Omega})$, and a spectral shape, $\bar{H}(f) \equiv (f/f_0)^\beta$, parameterized by the spectral index β and reference frequency f_0 . We set $f_0 = 100$ Hz to be in the sensitive range of the LIGO interferometers.

We measure $\mathcal{P}(\hat{\Omega})$ for two power-law signal models. In the cosmological model, $\beta = -3$ ($\Omega_{\text{GW}}(f) = \text{const}$), which is predicted, e.g., for the amplification of vacuum fluctuations following inflation [15]. In the astrophysical model, $\beta = 0$ ($\bar{H}(f) = \text{const}$), which emphasizes the strain sensitivity of the LIGO detectors.

We estimate $\mathcal{P}(\hat{\Omega})$ two ways. The *radiometer algorithm* [13,16,17] assumes the signal is a point source characterized by a single direction $\hat{\Omega}_0$ and amplitude, $\eta(\hat{\Omega}_0)$:

$$\mathcal{P}(\hat{\Omega}) \equiv \eta(\hat{\Omega}_0) \delta^2(\hat{\Omega}, \hat{\Omega}_0). \quad (2)$$

It is applicable to a GW sky dominated by a limited number of widely separated point sources. As the number of point sources is increased, however, the beam pattern will cause

the signals to interfere and partly cancel. Thus, radiometer maps do not apply to extended sources. Since pointlike signals are expected to arise from astrophysical sources, we use $\beta = 0$ for the radiometer analysis.

The *spherical-harmonic decomposition algorithm* is used for both $\beta = -3$ and $\beta = 0$. It allows for an extended source with an arbitrary angular distribution, characterized by spherical-harmonic coefficients \mathcal{P}_{lm} such that

$$\mathcal{P}(\hat{\Omega}) \equiv \sum_{lm} \mathcal{P}_{lm} Y_{lm}(\hat{\Omega}). \quad (3)$$

The series is cut off at l_{max} , allowing for angular scale $\sim 2\pi/l_{\text{max}}$. The flexibility of the spherical-harmonic algorithm comes at the price of somewhat diminished sensitivity to point sources, and thus the algorithms are complementary.

We choose l_{max} to minimize $\sigma(\hat{\Omega})\bar{A}$ where $\sigma(\hat{\Omega})$ is the uncertainty associated with $\mathcal{P}(\hat{\Omega})$ and \bar{A} is the typical angular area of a resolved patch of sky [18]. I.e., we maximize the sensitivity obtained by integrating over the typical search aperture. We thereby obtain $l_{\text{max}} = 7$ and 12 for $\beta = -3$ and $\beta = 0$, respectively.

Both algorithms can be framed in terms of a “dirty map”, X_ν , which represents the signal convolved with the Fisher matrix, $\Gamma_{\mu\nu}$ [14]:

$$X_\nu = \sum_{ft} \gamma_\nu^*(f, t) \frac{\bar{H}(f)}{P_1(f, t)P_2(f, t)} C(f, t) \quad (4)$$

$$\Gamma_{\mu\nu} = \sum_{ft} \gamma_\mu^*(f, t) \frac{\bar{H}^2(f)}{P_1(f, t)P_2(f, t)} \gamma_\nu(f, t). \quad (5)$$

Here both Greek indices μ and ν take on values of lm for the SHD algorithm and $\hat{\Omega}$ for the radiometer algorithm. $C(f, t)$ is the cross spectral density generated for each interferometer pair. $P_1(f, t)$ and $P_2(f, t)$ are the individual power spectral densities, and $\gamma_\mu(f, t)$ is the angular decomposition of the overlap reduction function $\gamma(\hat{\Omega}, f, t)$, which characterizes the orientations and frequency response of the detectors [14]:

$$\gamma_\mu(f, t) \equiv \int_{S^2} d\hat{\Omega} \gamma(\hat{\Omega}, f, t) \mathbf{e}_\mu(\hat{\Omega}) \quad (6)$$

$$\gamma(\hat{\Omega}, f, t) = \frac{1}{2} F_1^A(\hat{\Omega}, t) F_2^A(\hat{\Omega}, t) e^{i2\pi f \hat{\Omega} \cdot (\Delta \vec{x}_{12}(t))/c}. \quad (7)$$

$F_I^A(\hat{\Omega}, t)$ characterizes the detector response of detector I to a GW with polarization A , $\mathbf{e}_\mu(\hat{\Omega})$ is a basis function, c is the speed of light and $\Delta \vec{x}_{12} \equiv \vec{x}_1 - \vec{x}_2$ is the difference vector between the interferometer locations [14].

In [14] it was shown that the maximum-likelihood estimators of GW power are given by $\hat{\mathcal{P}} = \Gamma^{-1}X$. The inversion of Γ is complicated by singular eigenvalues associated with modes to which the Hanford-Livingston (HL) detector

network is insensitive. This singularity can be handled two ways. The radiometer algorithm assumes the signal is pointlike, implying that correlations between neighboring pixels can be ignored. Consequently, we can replace Γ^{-1} with $(\Gamma_{\hat{\Omega}\hat{\Omega}})^{-1}$ to estimate the point source amplitude $\eta(\hat{\Omega})$.

The SHD algorithm targets extended sources, so the full Fisher matrix must be taken into account. We regularize Γ by removing a fraction \mathcal{F} of the modes associated with the smallest eigenvalues, to which the HL network is relatively insensitive. By removing some modes from the Fisher matrix, we obtain a regularized inverse Fisher matrix, Γ_R^{-1} , thereby introducing a bias discussed below.

We thereby obtain estimators

$$\hat{\eta}_{\hat{\Omega}} = (\Gamma_{\hat{\Omega}\hat{\Omega}})^{-1} X_{\hat{\Omega}} \quad (8)$$

$$\hat{\mathcal{P}}_{lm} = \sum_{l'm'} (\Gamma_R^{-1})_{lm,l'm'} X_{l'm'}, \quad (9)$$

with uncertainties

$$\sigma_{\hat{\Omega}}^{\text{rad}} = (\Gamma_{\hat{\Omega}\hat{\Omega}})^{-1/2} \quad (10)$$

$$\sigma_{lm}^{\text{sph}} = [(\Gamma_R^{-1})_{lm,lm}]^{1/2}. \quad (11)$$

We refer to $\hat{\mathcal{P}}_{\hat{\Omega}} \equiv \sum_{lm} \hat{\mathcal{P}}_{lm} Y_{lm}(\hat{\Omega})$ as the ‘‘clean map’’ and $\hat{\eta}_{\hat{\Omega}}$ as the ‘‘radiometer map.’’ $\hat{\mathcal{P}}_{\hat{\Omega}}$ has units of $\text{strain}^2 \text{Hz}^{-1} \text{sr}^{-1}$ whereas $\hat{\eta}_{\hat{\Omega}}$ has units of $\text{strain}^2 \text{Hz}^{-1}$.

In choosing \mathcal{F} , we balance the sensitivity to the kept modes with the bias associated with the removed modes. In practice, we do not know the bias associated with \mathcal{F} , which depends on the unknown signal distribution $\mathcal{P}(\hat{\Omega})$. Therefore, we choose \mathcal{F} to produce reliably reconstructed maps with minimal bias for simulated signals. Following [14], we use $\mathcal{F} = 1/3$, which was shown to be a robust choice for simulated signals including maps characterized by one or more point sources, dipoles, monopoles and an extended source clustered in the galactic plane.

The likelihood function for $\mathcal{P}(\hat{\Omega})$ at each point in the sky can be described as a normal distribution with mean $\hat{\mathcal{P}}_{\hat{\Omega}}$ and width $\sigma_{\hat{\Omega}}^{\text{sph}}$. Regularization introduces a signal-dependent bias. Without knowing the true distribution of $\mathcal{P}(\hat{\Omega})$, it is impossible to know the bias exactly, but it is possible to set a conservative upper limit by assuming that on average the removed modes contain no more GW power than the kept modes. Thus, we calculate $\hat{\mathcal{P}}_{lm}$ setting eigenvalues of removed modes to zero, whereas σ_{lm}^{sph} is conservatively calculated setting eigenvalues of removed modes to the average eigenvalue of the kept modes. These upper limits are $\approx 25\%$ greater than they would be if we used the same regularization scheme for σ_{lm}^{sph} and $\hat{\mathcal{P}}_{lm}$.

In the case of the SHD algorithm, we also calculate [14],

$$\hat{C}_l \equiv \frac{1}{2l+1} \sum_m [|\hat{\mathcal{P}}_{lm}|^2 - (\Gamma_R^{-1})_{lm,lm}], \quad (12)$$

which describe the angular scale of the clean map. The subtracted second term makes the estimator unbiased so that $\langle \hat{C}_l \rangle = 0$ when no signal is present. The noise distribution of \hat{C}_l is highly non-Gaussian for small values of l , and so the upper limits presented below are calculated numerically. The \hat{C}_l are analogous to similar quantities defined in the context of temperature fluctuations of the cosmic microwave background [19].

The analysis was performed blindly using the S5 stochastic analysis pipeline. This pipeline has been tested with hardware and software injections, and the successful recovery of isotropic hardware injections is documented in [12]. The recovery of anisotropic software injections is demonstrated in [14]. We parse time series into 60 s, Hann-windowed, 50%-overlapping segments, coarse-grained to achieve 0.25 Hz resolution. We apply a stationarity cut described in [13], which rejects $\sim 3\%$ of the segments. We also mask frequency bins associated with instrumental lines (e.g., harmonics of the 60 Hz power, calibration lines and suspension-wire resonances) as well as injected, simulated pulsar signals. For $\beta = -3, 0$ we include frequency bins up to 200, 500 Hz, so that $\sigma(\hat{\Omega})$ is within $\leq 2\%$ of the minimum possible value. Thirty-three frequency bins are masked, corresponding to 2% of the frequency bins between 40–500 Hz used in the broadband analyses.

In order to determine if there is a statistically significant GW signature, we consider the highest signal-to-noise ratio (SNR) frequency bin or sky-map pixel. We calculate the expected noise probability distribution of the maximum SNR given many independent trials (in a spectral band) and given many *dependent* trials (for a sky map).

For N independent frequency bins, the probability density function, $\pi(\rho_{\text{max}})$, of maximum SNR, ρ_{max} , is

$$\pi(\rho_{\text{max}}) \propto [1 + \text{erf}(\rho_{\text{max}}/\sqrt{2})]^{N-1} e^{-\rho_{\text{max}}^2/2}. \quad (13)$$

The Gaussianity of $\hat{\mathcal{P}}_{\hat{\Omega}}$ and $\hat{\eta}_{\hat{\Omega}}$, calculated by summing over many $\mathcal{O}(500 \text{ K})$ independent segments, is expected to arise due to the central limit theorem [20]. Additionally, we find the Gaussian-noise hypothesis to be consistent with time-slide studies, wherein we perform the cross-correlation analysis with unphysical time shifts in order to wash out astrophysical signals and thereby obtain different realizations of detector noise.

The distribution of maximum SNR for a sky map is more subtle due to the nonzero covariances between estimators for different patches on the sky. For this case, we calculate $\pi(\rho_{\text{max}})$ numerically by simulating many realizations of dirty maps with covariances described by the Fisher matrix Γ .

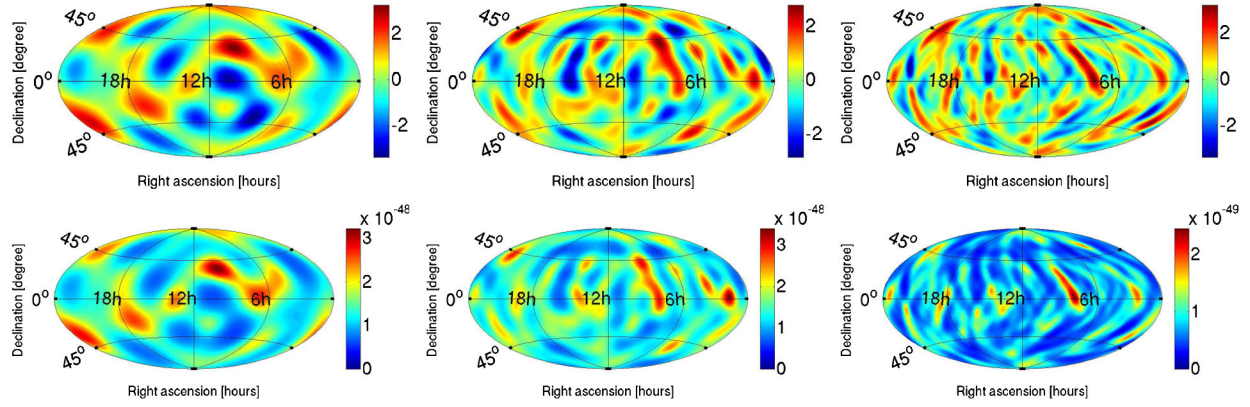


FIG. 1 (color online). Top row: SNR maps for the three different analyses: SHD clean map $\beta = -3$ (left), SHD clean map $\beta = 0$ (center), and radiometer $\beta = 0$ (right). All three SNR maps are consistent with detector noise. The p values associated with each map's maximum SNR are (from left to right) $p = 25\%$, $p = 56\%$, $p = 53\%$. Bottom row: The corresponding 90% C.L. upper-limit maps on strain power in units of $\text{strain}^2 \text{Hz}^{-1} \text{sr}^{-1}$ for the SHD algorithm, and units of $\text{strain}^2 \text{Hz}^{-1}$ for the radiometer algorithm.

Following [12], we marginalize over the H1, H2, and L1 calibration uncertainties [12], which were measured to be 10%, 10%, and 13%, respectively [21]. Using a prior, taken to be flat above $\mathcal{P}(\hat{\Omega}) = 0$, we obtain Bayesian upper limits at 90% C.L. [22].

Results.—Figure 1 shows sky maps for SHD $\beta = -3$ (left), SHD $\beta = 0$ (center), and the radiometer $\beta = 0$ (right). The top row contains SNR maps. The maximum SNR values are 3.1 (with significance $p = 25\%$), 3.1 ($p = 56\%$), and 3.2 ($p = 53\%$), respectively. These p values take into account the number of search directions and covariances between different sky patches. Observing no evidence of GWs, we set upper limits on GW power. The 90% confidence level (C.L.) upper-limit maps are given in the bottom row. For SHD $\beta = -3$, the limits are between $5 - 31 \times 10^{-49} \text{ strain}^2 \text{Hz}^{-1} \text{sr}^{-1}$; for SHD $\beta = 0$, the limits are between $6 - 35 \times 10^{-49} \text{ strain}^2 \text{Hz}^{-1} \text{sr}^{-1}$; and for the radiometer $\beta = 0$, the limits are between $2 - 20 \times 10^{-50} \text{ strain}^2 \text{Hz}^{-1}$. Since the radiometer and SHD maps have different units— $\text{strain}^2 \text{Hz}^{-1}$ and $\text{strain}^2 \text{Hz}^{-1} \text{sr}^{-1}$ respectively—one must scale the SHD map by the typical diffraction limited resolution $\bar{A} \approx 0.1 \text{ sr}$ to perform an approximate comparison.

The strain power limits can also be expressed in terms of energy flux per unit frequency [13]:

$$\hat{F}(f, \hat{\Omega}) = \left(3.18 \times 10^{42} \frac{\text{erg}}{\text{cm}^2 \text{s}}\right) \left(\frac{f}{100 \text{ Hz}}\right)^{\beta+2} \hat{\mathcal{P}}_{\hat{\Omega}}. \quad (14)$$

(Radiometer energy flux is obtained by replacing $\hat{\mathcal{P}}_{\hat{\Omega}}$ with $\hat{\eta}_{\hat{\Omega}}$.) The corresponding values are $2 - 10 \times 10^{-6} (f/100 \text{ Hz})^{-1} \text{ erg cm}^{-2} \text{s}^{-1} \text{Hz}^{-1} \text{sr}^{-1}$ and $2 - 11 \times 10^{-6} (f/100 \text{ Hz})^2 \text{ erg cm}^{-2} \text{s}^{-1} \text{Hz}^{-1} \text{sr}^{-1}$ for the SHD method, and $6 - 60 \times 10^{-8} (f/100 \text{ Hz})^2 \text{ erg cm}^{-2} \text{s}^{-1} \text{Hz}^{-1}$ for the radiometer. The radiometer limits constitutes a factor of ~ 30 improvement over the previous best [13].

Figure 2 shows 90% C.L. upper limits on the C_l . Since the $\hat{\mathcal{P}}_{\text{lm}}$ have units of $\text{strain}^2 \text{Hz}^{-1} \text{sr}^{-1}$, the C_l have the somewhat unusual units of $\text{strain}^4 \text{Hz}^{-2} \text{sr}^{-2}$.

Sco X-1 is a nearby (2.8 kpc) low-mass x-ray binary likely to include a neutron-star spun up through accretion. Its spin frequency is unknown. It has been suggested that the accretion torque is balanced by GW emission [23]. The Doppler line broadening due to the orbital motion is smaller than the chosen $\delta f = 0.25 \text{ Hz}$ bin width for frequencies below $\approx 930 \text{ Hz}$ [24]. At higher frequencies, the signal is certain to span two bins. We determine the maximum value of SNR in the direction of Sco X-1 to be 3.6 ($p = 73\%$ given $\mathcal{O}(7000)$ independent frequency bins) at $f = 1770.50 \text{ Hz}$. Thus in Fig. 3 (first panel) we present limits on root-mean-square (RMS) strain, $h_{\text{RMS}}(f, \hat{\Omega})$, as a function of frequency in the direction of Sco X-1 (RA, dec) = (16.3 hr, 15.6°). These limits improve on the previous best by a factor of ~ 5 [13]. RMS strain is related to narrow-band GW power via

$$h_{\text{RMS}}(f, \hat{\Omega}) = [\eta(f, \hat{\Omega}) \delta f]^{1/2}, \quad (15)$$

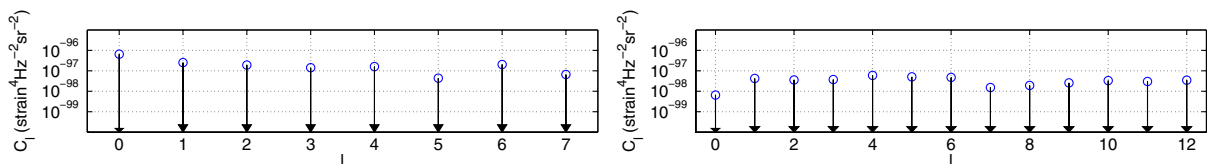


FIG. 2 (color online). Upper limits on C_l at 90% CL vs l for the SHD analyses for $\beta = -3$ (left) and $\beta = 0$ (right). The \hat{C}_l are consistent with detector noise.

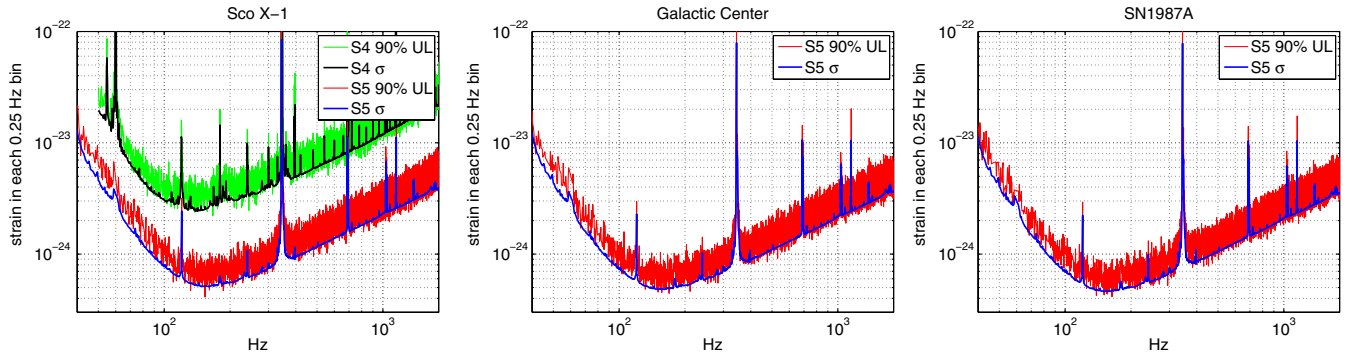


FIG. 3 (color online). Radiometer 90% upper limits on RMS strain in each 0.25 Hz wide bin as a function of frequency for Sco X-1 (top-left), the Galactic center (top-right) and SN 1987A (bottom). The large spikes correspond to harmonics of the 60 Hz power mains, calibration lines and suspension-wire resonances. The previous S4 upper limits for Sco X-1 [13] are also plotted in the top-left panel, illustrating the improvement in the upper limits obtained by using the LIGO S5 data. This is the first radiometer measurement of the Galactic center and SN 1987A.

and is better suited for comparison with searches for periodic GWs [25] (see also [26]). These limits apply to a circularly polarized signal from a pulsar whose spin axis is aligned with the line of sight. The limits constrain the RMS strain in each bin as opposed to the total RMS strain from Sco X-1, which might span two bins.

We also look for statistically significant signals associated with the Galactic center (RA, dec) = (17.8 hr, -29°) and SN 1987A (RA, dec) = (5.6 hr, -69°). The maximum SNR values are 3.5 ($p = 85\%$) at $f = 203.25$ Hz and 4.3 at ($p = 7\%$) 1367.25 Hz, respectively. Limits on RMS strain are given in Fig. 3.

In summary, no evidence was found to support the detection of either extended or pointlike GW sources. However, the clean maps in Fig. 1 represent the first effort to look for anisotropic extended sources of GWs. With the ongoing construction of second-generation GW interferometers [27–30], we expect to achieve strain sensitivities that will test plausible astrophysical and cosmological models. The new framework presented here is expected to serve as the paradigm for future stochastic analyses.

The authors gratefully acknowledge the support of the United States National Science Foundation for the construction and operation of the LIGO Laboratory, the Science and Technology Facilities Council of the United Kingdom, the Max-Planck-Society, and the State of Niedersachsen/Germany for support of the construction and operation of the GEO600 detector, and the Italian Istituto Nazionale di Fisica Nucleare and the French Centre National de la Recherche Scientifique for the construction and operation of the Virgo detector. The authors also gratefully acknowledge the support of the research by these agencies and by the Australian Research Council, the International Science Linkages program of the Commonwealth of Australia, the Council of Scientific and Industrial Research of India, the Istituto Nazionale di

Fisica Nucleare of Italy, the Spanish Ministerio de Educación y Ciencia, the Conselleria d’Economia Hisenda i Innovació of the Govern de les Illes Balears, the Foundation for Fundamental Research on Matter supported by the Netherlands Organisation for Scientific Research, the Polish Ministry of Science and Higher Education, the FOCUS Programme of Foundation for Polish Science, the Royal Society, the Scottish Funding Council, the Scottish Universities Physics Alliance, The National Aeronautics and Space Administration, the Carnegie Trust, the Leverhulme Trust, the David and Lucile Packard Foundation, the Research Corporation, and the Alfred P. Sloan Foundation.

*ethrane@physics.umn.edu

- [1] E. W. Kolb and M. S. Turner, *The Early Universe* (Westview Press, Boulder, CO, 1994).
- [2] A. A. Starobinskii, *JETP Lett.* **30**, 682 (1979).
- [3] T. W. B. Kibble, *J. Phys. A* **9**, 1387 (1976).
- [4] A. Buonanno, M. Maggiore, and C. Ungarelli, *Phys. Rev. D* **55**, 3330 (1997).
- [5] R. Brustein, M. Gasperini, M. Giovannini, and G. Veneziano, *Phys. Lett. B* **361**, 45 (1995).
- [6] E. Howell *et al.*, *Mon. Not. R. Astron. Soc.* **351**, 1237 (2004).
- [7] V. Ferrari, S. Matarrese, and R. Schneider, *Mon. Not. R. Astron. Soc.* **303**, 258 (1999).
- [8] T. Regimbau and B. Chauvineaux, *Classical Quantum Gravity* **24**, S627 (2007).
- [9] T. Regimbau and J. A. de Freitas Pacheco, *Astron. Astrophys.* **376**, 381 (2001).
- [10] B. P. Abbott *et al.*, *Rep. Prog. Phys.* **72**, 076901 (2009).
- [11] B. Abbott *et al.*, *Astrophys. J. Lett.* **683**, L45 (2008).
- [12] B. Abbott *et al.*, *Nature (London)* **460**, 990 (2009).
- [13] B. Abbott *et al.*, *Phys. Rev. D* **76**, 082003 (2007).
- [14] E. Thrane *et al.*, *Phys. Rev. D* **80**, 122002 (2009).

- [15] M. Maggiore, *Phys. Rep.* **331**, 283 (2000).
- [16] S.W. Ballmer, *Classical Quantum Gravity* **23**, S179 (2006).
- [17] S. Mitra, S. Dhurandhar, T. Souradeep *et al.*, *Phys. Rev. D* **77**, 042002 (2008).
- [18] The data were first processed with $l_{\max} = 20$; the present method of choosing l_{\max} was then adopted *a posteriori* to more accurately model the network's angular resolution.
- [19] G. Hinshaw *et al.*, *Astrophys. J. Suppl. Ser.* **180**, 225 (2009).
- [20] B. Allen and J.D. Romano, *Phys. Rev. D* **59**, 102001 (1999).
- [21] We follow the marginalization scheme used in [12], but note that this does not take into account covariance between baselines with a shared detector. Because the H2L1 baseline only contributes about 10% of the sensitivity, and the calibration uncertainty is on the order of 10% to start with, this effect is only on the order of 1%.
- Work is ongoing to take this effect into account.
- [22] A prior constructed from [13] would be nearly flat anyway since the strain sensitivity has improved 10-fold since S4.
- [23] D. Chakrabarty *et al.*, *Nature (London)* **424**, 42 (2003).
- [24] D. Steeghs and J. Casares, *Astrophys. J.* **568**, 273 (2002).
- [25] B. Abbott *et al.*, *Phys. Rev. D* **76**, 082001 (2007).
- [26] C. Messenger, *Understanding the Sensitivity of the Stochastic Radiometer Analysis in Terms of the Strain Tensor Amplitude*, LIGO Document T1000195-v1 (2010).
- [27] G. Harry for LIGO Science Collaboration, *Classical Quantum Gravity* **27**, 084006 (2010).
- [28] J.R. Smith for LIGO Science Collaboration, *Classical Quantum Gravity* **26**, 114013 (2009).
- [29] F. Acernese for Virgo Collaboration, *Classical Quantum Gravity* **23**, S63 (2006).
- [30] K. Kuroda for LCGT Collaboration, *Classical Quantum Gravity* **27**, 084004 (2010).